Bull. Chem. Soc. Jpn., 70, 2619—2629 (1997)

Headline Articles

Theoretical Prediction of Intracluster Reactions of $B^+(H_2O)_2$ and $B^+(H_2O)_3$: Hybrid Procedure of Ab Initio MO Calculations and Monte Carlo Samplings

Hidekazu Watanabe, Toshio Asada, and Suehiro Iwata*

Graduate University for Advanced Studies and Institute for Molecular Science, Okazaki 444

(Received May 22, 1997)

A recently developed hybrid procedure of ab initio molecular orbital (MO) calculations and Monte Calro (MC) samplings is applied to investigate the intracluster reactions of $B^+(H_2O)_n$ ($n=2$ and 3). In this procedure we do not assume the potential energy functions during MC samplings. At every step the ab initio MO method is directly used to evaluate the electronic energy. The procedure makes it possible to deal with the intra-cluster reaction involving any rearrangement of atoms such as isomerization and dissociation. The many-body effects on the energy are taken into account within the approximation used in the MO calculation. During the MC samplings at room temperature, the $B^+(H_2O)_2$ cluster undergoes a series of isomerization reactions, and eventually forms the most stable isomer, sp^2 type of *trans* $HBOH^+(H_2O)$. For $B^+(H_2O)_3$, the reactions turn out to be more complicated, and a few times simulations suggest that there are several reaction products as well as intermediates in the reactions. The MO-MC procedure is proved to be a powerful tool to search for many isomers, reaction intermediates, and the products as well as the transition state structures between them although it is still very time-consuming.

Hydrated clusters $X(H_2O)_n$ and their ions $X^+(H_2O)_n$ and $X^-(H_2O)_n$ are among the most well-examined systems in cluster chemistry and physics. Thanks to recent advances in molecular beam techniques combined with the time-of-flight (TOF) mass spectroscopy, the size-controlled hydrated clusters have been experimentally examined for various solute molecules, X. In particular, for the group 1, 2, and 3 elements and their cations, Fuke, Duncan, Hertel, Lisy, Farrar, and others[1—21] have studied the intracluster reactions and photo-absorption and photo-dissociation processes. Fuke and his coworkers reported the TOF studies on $Al^+(H_2O)_n$ clusters,[1—3] and found size-dependent reactions and photochemistry. In contrast, there are almost no experimental studies on $B^+(H_2O)_n$, probably because of the high ionization energy of a boron atom. From the theoretical side, it is also true; there are many reports, including ours, on $Al^+(H_2O)_n$,[22—26] but very few on $B^+(H_2O)_n$. Very recently we reported ab initio MO calculations of both $Al^+(H_2O)_n$ and $B^+(H_2O)_n$, and compared their geometric structures.[26] In that paper, we also enumerated the possible isomers of both ions, and showed that the boron ion is much more reactive than the aluminum ion. We found that, if a boron ion collides with water clusters even at less than thermal energy, the intracluster reactions might proceed. Our work, however, was very static; we only determined the geometric structures of the isomers, and we could not locate the transition state structures between the isomers, and therefore, could not determine the barrier height of the isomerization reactions. The present work is an extension of the previous work with a new theoretical equipment recently developed by us.

The Monte Carlo (MC) simulations[27—30] have been used to study the thermochemical properties of various macroscopic systems such as liquids and solutions, polymers, surfaces and solids. The MC method has recently been applied to cluster science. The MC method has both advantages and disadvantages against the molecular dynamics (MD), which becomes powerful by being combined with the ab initio plane-wave based density functional theory in the Car–Parinello method.[31] Very recently we developed a hybrid computational procedure of the conventional ab initio MO calculations with the Monte-Carlo (MC) samplings, and applied it to the study of the clusters of $Mg^+(H_2O)_n$ ($n=1$—4).[32] The MO-MC method is also applied to $B^+(H_2O)$.[33] In both cases, some of thermal properties and structural fluctuations are found, but the intracluster reactions do not proceed at the temperature assumed in the calculations, though a few clues of the reactions are observed in the radial distributions and charge fluctuations. In the present paper, we will report the

application of the method to $B^+(H_2O)_2$ and $B^+(H_2O)_3$. In our previous work, we found several isomers having chemical formulae $[BH_4O_2]^+$ and $[BH_6O_3]^+$. In the present paper, armed with the new MO-MC procedure, we examine the reaction processes to more stable isomers and the dissociation processes. Finally we will discuss the prospects of the stability and reactivity of the $B^+(H_2O)_n$ system.

Method

The computational procedures are essentially the same as in the previous studies for $Mg^+(H_2O)_n$ and $B^+(H_2O)$.[32,33] Here we briefly describe several new features in the hybrid procedure of ab initio MO-MC samplings. The most important characteristic in the present method is not to use any empirical nor semi-empirical potential functions, and instead to directly calculate the electron energy at every step with the ab initio MO method. Therefore, the approximation for the energy calculation is determined by the basis functions and the form of the many-electron wave function. The many-body interaction is explicitly taken into consideration within the approximation of the many-electron wave function used. In the present study, since the clusters $B^+(H_2O)_n$ are even electron systems, the closed shell SCF wave function is a good approximation for stable structures, and the electron correlation effects, examined in the previous work, are not large, particularly on the structures. Within this approximation, we can treat the intra-cluster reaction which involves the rearrangement of arbitrary atoms. Of course, care should be taken about the bond breaking. We will discuss on the advantage of the MC samplings over the MD simulation in tracing the bond breaking reactions.

To trace the intracluster reaction mentioned above, we have to allow all atoms to move independently at every step of MC sampling (we may call them non-rigid moves) in principle. But, it is very inefficient and the acceptance rate is expected to be small. The molecular units in the cluster are easily identified in the present system; if one of the units is broken, the energy becomes high and the move is usually not accepted in the Metropolis sampling, but importantly it can be sometimes accepted. So as to increase the efficiency and simultaneously to allow the rearrangement of the molecular units, we have introduced two types of moves; one is the non-rigid move and the other is the rigid move. In the latter, the molecular unit is determined by the interatomic distances (cluster analysis method).[34] In most simulations, 1.3 Å is used for the threshold distance in determining the unit. The choice of the non-rigid or rigid move is determined at random. The ratio of the non-rigid to rigid moves is controlled to be close to 50%. This ratio is in some sense arbitrary, and the samplings are biased to the intracluster reactions. By introducing the two types of moves with nearly equal weights, we are able to significantly broaden the configuration space we can visit in a limited number of samplings.

Once a move is selected, the usual Metropolis sampling technique is employed. The temperature of MC sampling is 300 K throughout the present paper. Here, the care should be taken for the meaning of the temperature in such an isolated system as we study in the present paper. The ratio $\Delta E/kT$ in the Metropolis samplings, where the temperature appears, determines the amount of the energy fluctuation in the system. The use of the Metropolis samplings also implies that we assume the canonical ensemble for the clusters. It is certain that each cluster in the molecular beam is not under canonical condition. At the same time, we cannot assume microcanonical ensemble with a constant internal energy for clusters in the molecular beam. In the present study, we adopt the canonical distribution with an energy fluctuation to search the broad range of the configuration space.

The approximation level used in the ab initio MO calculation is SCF/6-31+G*. The basis set super position error (BSSE)[35] of the SCF/6-31+G* approximation was examined in the previous works.[26,32,33] The maximum displacement is adjusted during the samplings to give an acceptance ratio of close to 50%. To achieve this requirement, the maximum displacement in the non-rigid move is about 0.5 Å, and the maximum displacement and the maximum rotation angle in the rigid move are about 1.0 Å and 3.0°, respectively.

The programs used for ab initio MO calculations are GAUSSIAN 92 and GAUSSIAN 94 packages.[36,37] The computation was carried out on our workstations and on an IBM SP2 of the computer center of the Institute for Molecular Science.

Results and Discussion

The Reactions of $B^+(H_2O)_2$ and the Transition State Structures : In the previous work, we have found structures of four isomers of $B^+(H_2O)_2$ with ab initio MO calculations.[26] Figure 1 shows the structures of all four isomers, re-optimized with the SCF/6-31+G* level of approximation. The values under the structures are the relative energy differences among the isomers. The relative energy and the geometric parameters determined in these calculations are not much different from those determined in the previous work with the SCF/6-31G* level. The isomer **2-1** has two water molecules which are directly bound to a boron ion B^+. In contrast, in the isomer **2-2**, only an oxygen of OH is directly bound to a B atom, forming a BOH molecule, and an oxionium ion H_3O^+ is hydrogen-bonded to it. This isomer is regarded as a proton-transferred product $BOH(H_3O)^+$ from $B^+(H_2O)(H_2O)$. The isomers **2-3** and **2-4** are the insertion reaction products of a O–H bond of a water molecule. In the isomer **2-3**, the $HBOH^+$ molecular ion core has the sp hybridization of a boron atom, while in the isomer **2-4**, the $HBOH^+$ molecular ion core is bent and the boron atom is sp^2 hybridized. Interestingly, without a hydrating water molecule, the linear $HBOH^+$ is more stable than the bent trans $HBOH^+$; the latter is not at the stationary point.[26]

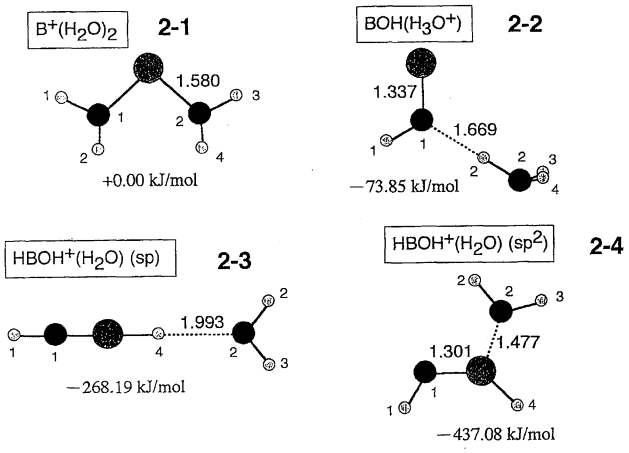

Fig. 1. Geometric structures of the isomers of $[B(H_2O)_2]^+$ and the relative energies. The numbers given to the isomers are used in text, figures and tables.

When we started performing the ab initio MO-MC samplings, we knew the structures of these four isomers as preliminary knowledge. However, the transition state structures connecting the isomers are not known. In the MC samplings, the initial conditions are very important, though not as much as in the classical molecular dynamics, in which everything which follows is determined by the initial conditions under classic mechanics. Because we are interested in whether the MO-MC hybrid method can follow the intracluster reactions, we have decided to start from the least stable structure **2-1** among the four isomers.

Reaching Thermal Equilibrium at the Most Stable Isomer : Figure 2a shows the energy profile along the MC samplings for $B^+(H_2O)_2$. The temperature at the MC samplings is 300 K. The energy parameter in the Metropolis samplings is 2.49 kJ mol^{-1}. We have calculated up to the 26000th step. Up to about the 5000th step, the energy rises up and falls down repeatedly, and then the system gradually loses the potential energy. After about the 5000th step, the energy becomes nearly constant with a thermal fluctuation around the assumed temperature. In Fig. 2c, the scale of the ordinate after the 10000th step is expanded. In both figures the horizontal thick lines show the energy of the isomers in Fig. 1. In this MC sampling, the isomer **2-1** is transformed to the most stable isomer **2-4**. The isomerization reaction takes place under thermal fluctuations around 300 K (18.7 kJ mol^{-1}).

The snapshots during the present MC sampling are shown in Fig. 2b. The thin vertical dotted lines and numbers (i, ii,,,) in Figs. 2a, 2c, and 2d show their corresponding step numbers in Fig. 2b. At the 1024th step (structure (i)), the system reaches the highest energy; the oxygen (2) in one of water molecules moves away from the boron ion B^+ and approaches to a hydrogen of the other water molecule. At the 1673rd step (ii), two water molecules form a chain structure, but do not yet form the proton-transferred structure like isomer **2-2** in Fig. 1. The proton transfer reaction completes before the 1950th step (iii); the structure at the 1950th step is somewhat similar to isomer **2-2**. After this, the oxionium ion moves away from the BOH molecule (see the 2410th step (iv)), and it rotates to the other side of BOH, and is bound to the boron atom of BOH molecule (the 2688th step (v)). At the 3550th step (vi), the oxionium ion is bound to the boron atom of the BOH molecule, and the system becomes $HOB–H_3O^+$, which is not found to be at a local minimum on the global potential energy surface. In the present run of the MC samplings, the isomerization reaction from structure **2-2**, $BOH–OH_3^+$, to the most stable isomer **2-4**, the hydrated *cis* $HBOH^+$ complex with a water $HBOH^+–H_2O$, directly proceeds without visiting structure **2-3**, the sp type of a linear $HBOH^+$ complex. We have continued the samplings up to the 26000th step, as shown in Fig. 2d, but no more reactions are found. Consequently, we can conclude that after the 5000th step, the samplings reflect the thermal fluctuation of the sp^2 type of *cis*-$HBOH^+$ ion complex with a water molecule at 300 K. From the data we can evaluate some statistical properties of the canonical ensemble of the system, although the number of samplings is limited.

There is suggestive information in the energy profile and in the snapshots before the 5000th step, during which the isomerization reactions proceed. The profile has peaks and valleys. One may guess that the valleys are close to the local minima and the peaks are close to the transition states (TS) of the isomerization reactions. In fact, using structural information on the peaks, we have succeeded in finding the TS structures. Figure 3 shows the TS structures of the three steps of intracluster reactions of $B^+H_4O_2$. The structures of TS1 and TS2 are similar to the snapshots of the 1024th step (i) and 2410th step (iv), respectively, and are found by starting the search of the TS structures there. Because the present MC samplings have not yet reached structures close to the isomer **2-3**, the search for TS3 between isomers **2-3** and **2-4** has started from a structure between steps (vi) and (vii).

The energies of these TS structures are also shown in Fig. 2a by horizontal dotted lines. All barriers of intracluster reactions are very low: 8.8 kJ mol^{-1} for **2-1** to TS1, 11.4 kJ mol^{-1} for **2-2** to TS2, and only 1.6 kJ mol^{-1} for **2-3** to TS3. For the reverse reaction, on the other hand, the barrier is rather high; 82.4 kJ mol^{-1} for **2-2** to TS1, 205.9 kJ mol^{-1} for **2-3** to TS2, and 107.5 kJ mol^{-1} for **2-4** to TS3. This is the reason why the intra-cluster reactions proceed only one-way under thermal fluctuations of the room temperature.

After Reaching Thermal Equilibrium : After the 5000th step, the basic frame becomes the isomer **2-4**. We have taken the MC samples to the 26000 step. Assuming that the thermal equilibrium at 300 K is reached after the 6000th step, we evaluated some statistical properties. Figures 4a and 4b show the radial distributions of the bond distances of B–Os and B–Hs, and the distributions of the lengths of O–H and of the angles of B–O(1)–H(1) are shown in Figs. 4c and 4d. The numbering of atoms is shown in the inserted figure. In the distances of B–Hs and lengths of O–Hs, H(2) and H(3) are not differentiated in summing up the distribution. The integrated area is normalized to the total number of steps. The vertical dotted lines show the parameters for the optimized structure for **2-4**. Except for the radial distribution of B–H(4), the distributions deviate from the symmetric ones, though the peaks are somewhat close to the equilibrium distances. The exception is the radial distribution of the bond B–H(1), whose peak is substantially shorter than that of the equilibrium distance. In contrast, such a shift of the peak is not seen in the length O(1)–H(1). The special character of H(1) appears more clearly in the angle B–O(1)–H(1). The distribution of the angle has obviously two peaks. One peak is around the optimized geometry, and the other is at a much smaller angle than the former. The distribution of O(2)–Hs has also two peaks, but these two peaks are attributed to the slight difference of equilibrium bond distances of O(2)–H(2) and O(2)–H(3). The distributions of each of O(2)–H(2) and O(2)–H(3) are also shown in Fig. 4c with thin lines. The reason of the peculiarity for the hydrogen atom H(1) will be analysed further below. Figure 5 shows the distribution of Mulliken charge of all atoms after the 6000th

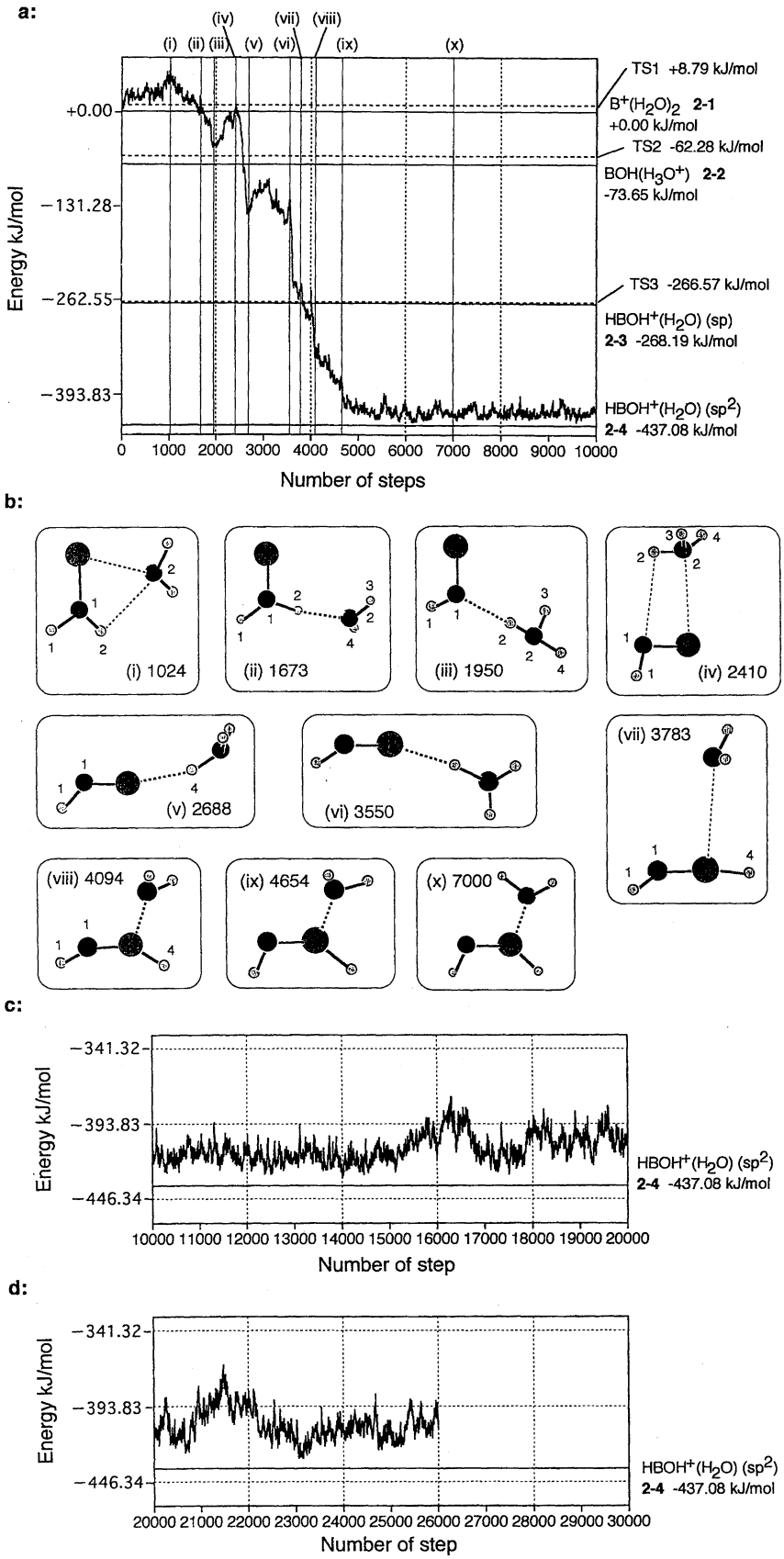

Fig. 2. The energy profile and structures of some intermediate steps. a) The energy profile till the 10000th step. The horizontal lines are the energy of the isomers (solid lines) and of the transition state structures (dotted lines). b) A series of snap shots at the steps indicated in (a) as vertical lines. c) The energy profile between the 10000th and the 20000th.step d) The energy profile after the 20000th step.

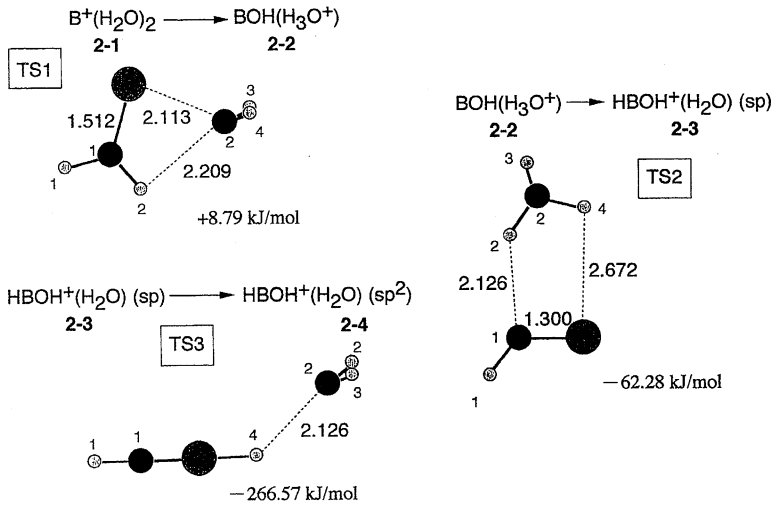

Fig. 3. The transition state structures for the intracluster reactions of $[B(H_2O)_2]^+$.

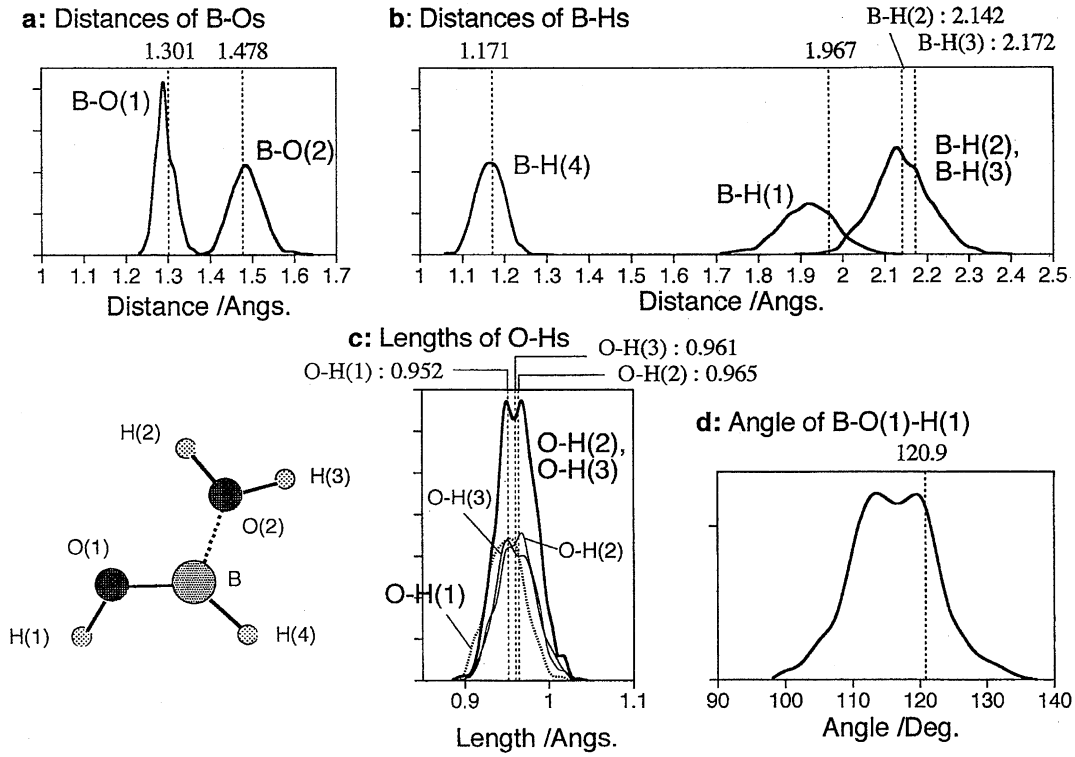

Fig. 4. The radial distributions after the 6000th to the 26000th step. a) Distances of B–Os. b) Distances of B–Hs c) Lengths of O–Hs d) Angle of B–O(1)–H(1). The numbering of the atoms are shown in the inserted picture. The area of each distribution is normalized to the total steps. The vertical lines are the parameters at the equilibrium geometry of **2-4**. The lower peak height implies the broader radial distribution. In b, two hydrogen atoms H(2) and H(3) are not distinguished in counting. In c, the distribution in which two hydrogen atoms are not distinguished are shown with the thick lines, and on the other hand, thin lines are those separately counted.

step. The widths of the charge distribution on boron and oxygen atoms are broad, while those on the hydrogen atoms are not great except for H(1). Similar trends are found in the case of $B^+(H_2O)$.[26] The vertical lines in the figure are the Mulliken charges of the equilibrium geometry. It is clear that all atoms except hydrogen H(4) becomes less charged than at the equilibrium geometry.

A closer look at the energy profile in Figs. 2c and d reveals that the average energy and the energy fluctuation slightly increase after the 15000th till the end of the samplings. To analyse the structure and dynamics of the isomer **2-4**, $(HOBH)^+(H_2O)$, the distributions are divided in two parts; from the 6000th to15000th step, and from the 15000th to 26000th step. We have noted above a peculiar radial distribution of the bond B–H(1) in Fig. 4 and a large charge fluctuation on H(1) in Fig. 5. A more enhanced characteristic

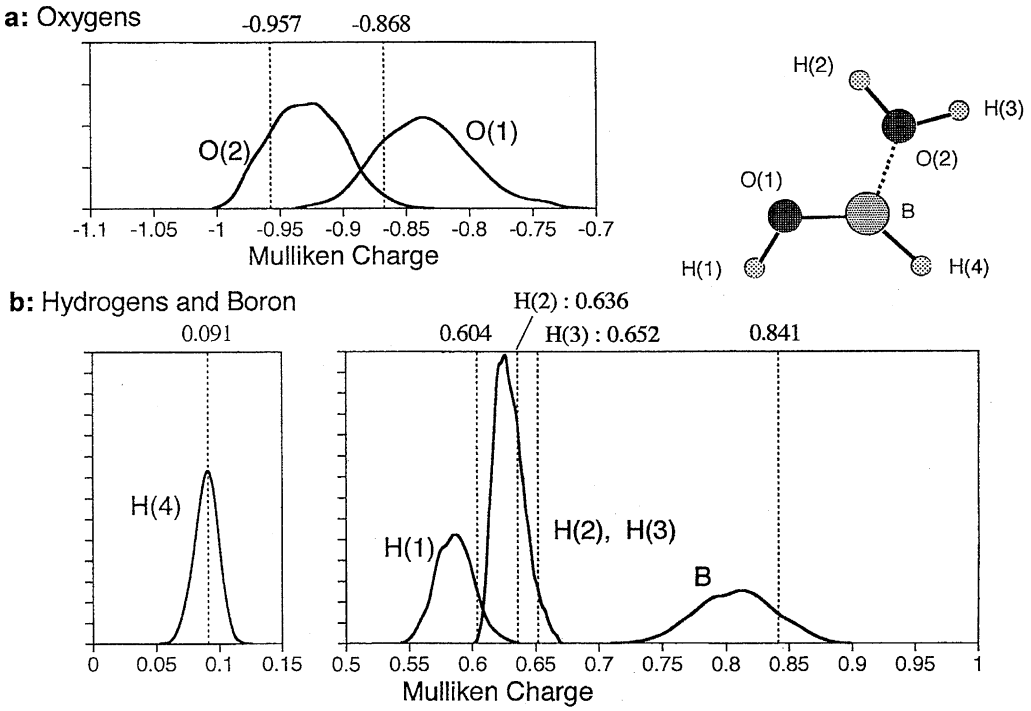

Fig. 5. The Mulliken charge distribution after the 6000th to the 26000th step. The distribution is normalized as in Fig. 4.

behavior of the hydrogen atom H(1) is seen in the distribution of angle B–O(1)–H(1) in Fig. 6c. The distribution from the 6000th to 26000th step has two peaks; when it is divided before and after the 15000th step, the two peaks are clearly separated. One of the peaks in these distributions is close to the corresponding value of the equilibrium geometry of **2-4**, and the other peak deviates from it. The length of O(1)–H(1) is an exception; the two distributions are similar to each other. One may consider that there is another local minimum near the optimized structure **2-4**. So we have tried to find

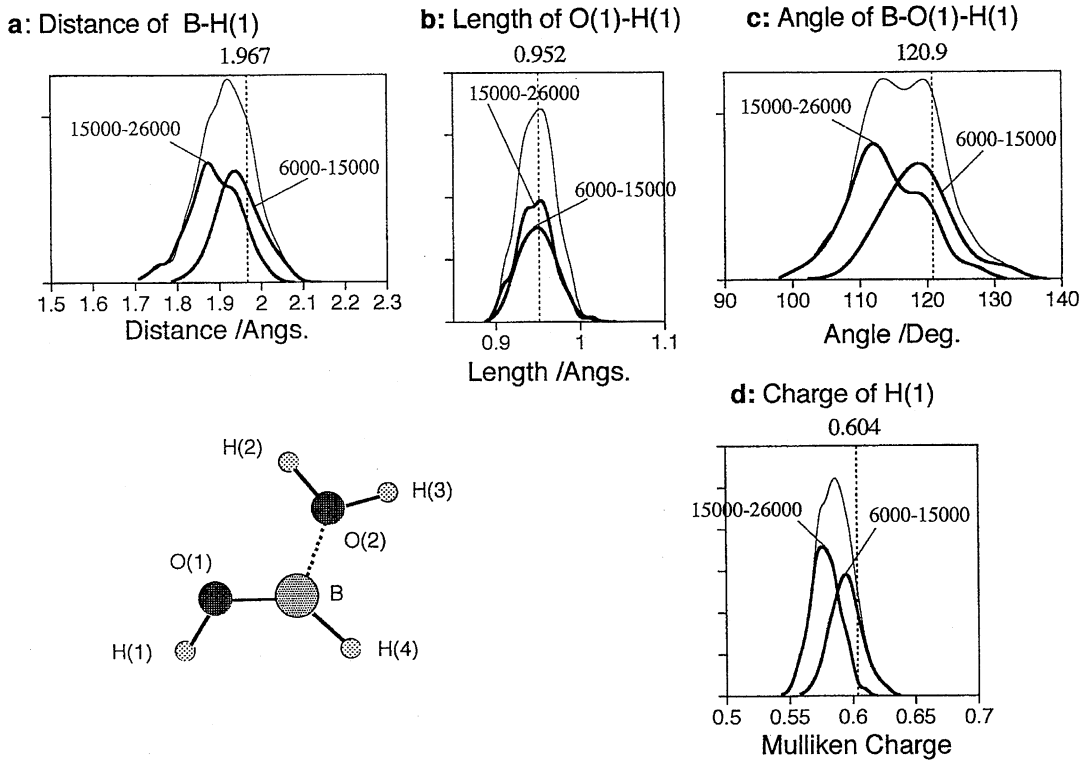

Fig. 6. The distributions of lengths B–H(1) and O(1)–H(1), angle B–O(1)–H(1), and Mulliken charge on H(1) from the 6000th to15000th step and from the 15000th to the 26000th step. The thin lines are the sum of two distributions.

it, but in vain. The region 15000–26000 is only due to the thermal fluctuations within available energies. The system is trapped in some kinds of valleys on the potential energy hyper-surface, where the slope to one or a few directions is weakly downward but to the most of the other directions is steeply upward. The valley might be on the way to a pass to the other reactions; that is, the large fluctuations in the angle and charge distributions are a symptom of some further intracluster reaction. One conceivable structure is *trans* type $HBOH^+(H_2O)$. The energy of *trans*-$HBOH^+(H_2O)$ is by +33.82 kJ mol^{-1} higher than that of *cis*-$HBOH^+(H_2O)$ at the SCF/6-31+G* level of approximation. By deducing from the shifts of the fluctuation peaks, the likely path of the hydrogen H(1) is the torsional motion to the *trans*-form. It is obvious that more extensive samplings and analyses are required to elucidate the possible reactions of the system. But we could emphasize the potentiality of the MO-MC procedure to find a new noble and unexpected reaction process.

$B^+(H_2O)_3$. Figure 7 shows the structures of all of the isomers of chemical formula $[BH_6O_3]^+$ we have found. They are all confirmed to be at local minima on the potential energy surface by evaluating the harmonic frequencies. To trace the model dynamics of the ion $[BH_6O_3]^+$, we have selected the isomers **3-1**, **3-2** and **3-5** for the initial geometries of MC samplings. In isomer **3-1**, all three water molecules are directly bound to a boron ion, and **3-1** is the least stable isomer. In isomer **3-2**, only two water molecules are in the first hydration shell. The third water is bound with both of the first shell water molecules, forming a six-membered ring. This six-membered ring is a stable hydrogen-bond network and is seen in several metallic ions with water clusters.[22,25,26,38—44] The isomer **3-5** has a hydrogen bond chain structure, and a product, $BOH(H_3O^+)H_2O$, of the proton transfer reaction. As is shown in Fig. 7, the energy differences among various chemical species of $[BH_6O_3]^+$ are rather large.

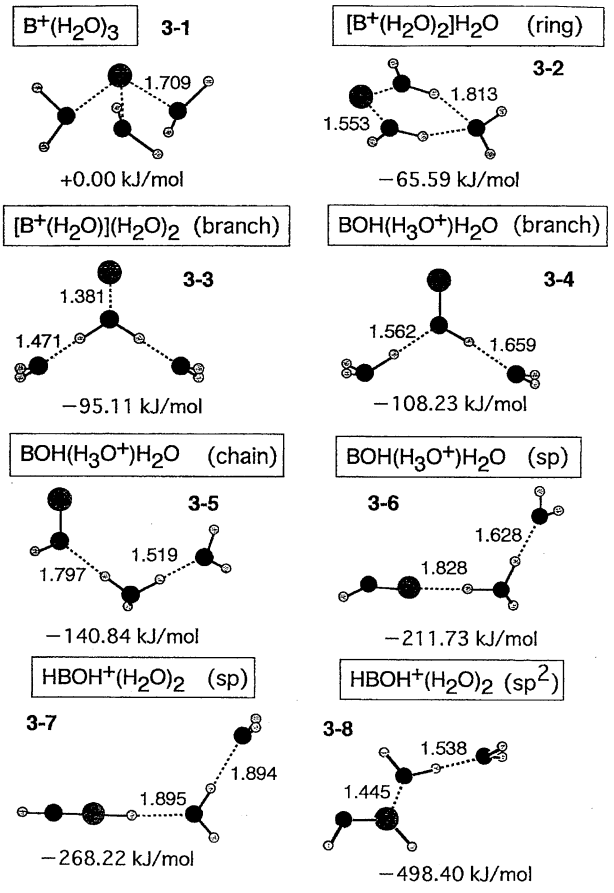

Fig. 7. Geometric structures of the isomers of $[B(H_2O)_3]^+$ and the relative energies. The numbers given to the isomers are used in text, figures and tables.

Starting from $B^+(H_2O)_3$ (Isomer 3-1): Figure 8a shows the energy profile along the MC samplings, which start from isomer **3-1**. A series of snapshots are shown in Fig. 8b. As is found in the previous study,[26] the bond lengths of the B^+ ion and O atoms are slightly longer than those of $B^+(H_2O)_2$, which is explained by the repulsive interaction among water molecules. Starting from this structure, one of B^+–O bonds immediately becomes longer (see the 501st step (i)), and then, another B^+–O bond starts to get longer (see the 940th step (ii)). The isomerization reaction proceeds to structures **3-3** (iii) and **3-4** (iv) without falling into the local minimum structure **3-2** of a six-membered ring. The highest point of the profile in this run is at the 940th step (ii), which might be close to the transition state structure from **3-1** to **3-3**. Between 2900 and 12000 steps, the system stays ether at **3-3** or **3-4** (in most of steps, at **3-4** with a core BOH molecule); the two structures are related with a proton transfer reaction. The structures are entropy-favored, because of the floppy motion of water(s) and oxionium ion. Eventually, after rather several changes of the hydrogen bond pairs and proton transfer (note that in the figure the numbering of atoms is kept by assuming the classical motion), an ion $HOBH^+$ is formed at (ix). Then, a water starts to leave the ion $HOBH^+(H_2O)$. So the final product is a hydrated ion $HOBH^+(H_2O)$ plus a water molecule. In terms of the energy it is very conceivable, because the exothermic energy of the reaction to the product, $HOBH^+(H_2O)+H_2O$, from the initial isomer **3-1** is as large as −389.27 kJ mol^{-1}.

Interestingly, the product ion $HOBH^+(H_2O)$ has a chemical formula $[B(H_2O)_2]^+$. In other words, if the mass spectroscopy is employed, no intra-cluster reactions can be noticed, and there are no ways to distinguish the reaction from the mere evaporation of a water molecule.

Starting from $[B^+(H_2O)_2]^+H_2O$ (Isomer 3-2). The isomer **3-2** has a six-membered ring of hydrogen bond network. For some other hydrated metallic ions, such as Mg^+ and Al^+, this type of isomer is the most stable. For the hydrated B^+ ion, as shown in Fig. 7, $[B^+(H_2O)_1]^+$ $(H_2O)_2$ (isomer **3-3**) is more stable than **3-2**. Figure 9(a) is the energy profile, and the snapshots along the steps are depicted in Fig. 9(b). Immediately after the samplings start, the six-membered ring is broken as (i). Then, another water (O1 in (ii)) bonded to the B^+ ion starts to leave it (ii), and once the water bonds to the second shell water (O3 in (ii)), the proton transfer takes place to yield $BOH–(HOH_2)^+(H_2O)$ as (iii). After the 2000th step, the unit of the system is essentially this form, and eventually two moieties are separated from each other.

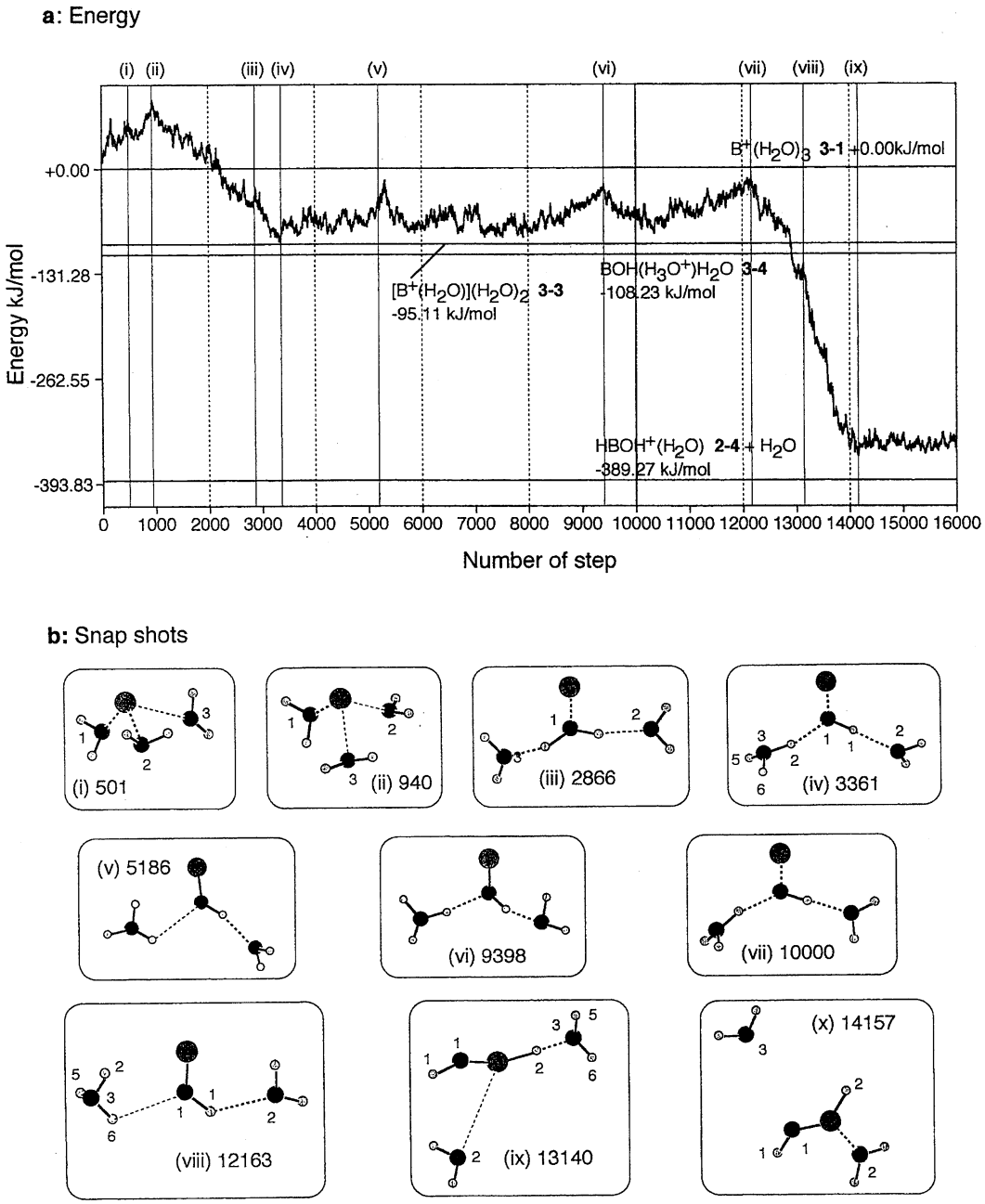

Fig. 8. Energy profile (a) and structures of some intermediate steps (b). The sampling starts at structure **3-1**, in which all three waters are bonded to the B^+ ion.

The energy of the dissociation limit (a horizontal bar at the left side of Fig. 9(a)) is well below the starting structure. In this run, apparently the boron cation is reduced to become a neutral BOH molecule and water molecules are oxidized to a hydrated oxionium ion.

Starting from $BOH(H_3O)^+H_2O$ (Isomer 3-5). The isomer **3-5** is a quenched structure from the plateau region between 2000 and 4000 in Fig. 9(a). In other words, if the geometry optimization with the energy gradient technique is carried out from these structures, eventually isomer **3-5** is reached as the minimum. In this structure the oxygen of BOH is a proton acceptor to the oxionium ion. Figure 10 shows the energy profile and a series of snapshots. At the 1703rd step, the oxionium is bonding to the boron side, but more steps are required to reach the structures similar to isomer **3-6**; The structure at the 7000th step (v) is very similar to **3-6**, having a colinear O–B—H. Then, suddenly after the12600th step the proton transfer reaction takes place to form a moiety $HBOH^+$ shown in (vii), which is similar to isomer **3-7**. Eventually the oxygen 2 moves to the positively charged boron, and almost simultaneously a water starts to evaporate. The product is the same one as that found in Fig. 8.

We have carried out only three runs for $[B(H_2O)_3]^+$, so that it can hardly be called "simulation of the intracluster reactions". Nevertheless, some important clues of the reactions are acquired by the MO-MC sampling procedure.

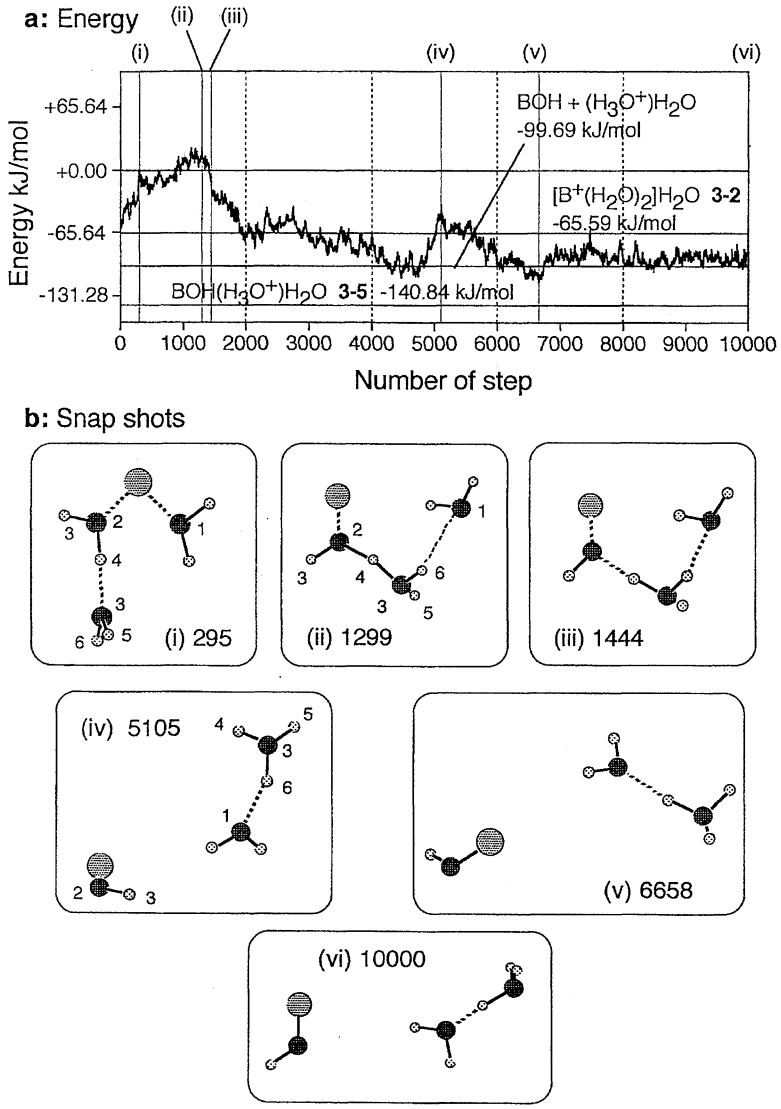

Fig. 9. Energy profile (a) and structures of some intermediate steps (b). The sampling starts at structure **3-2**, in which two waters are directly bonded to the B^+ ion.

Starting from two very different structures, we have reached the same product $HOBH^+(H_2O)+H_2O$. The similar reactions are expected for larger clusters $B^+(H_2O)_n$, because the core ion $HBOH^+$ is a very stable moiety. The product ion has a chemical form $B^+(H_2O)_n$, although the ion core is $HBOH^+$. This reminds us the second product switch observed for the reaction of M^+ (M = Mg or Ca) with water clusters $(H_2O)_n$. For small n, the mass spectra have peaks at the mass of $M^+(H_2O)_n$, but for intermediate sizes of n, the main product become $(MOH)^+(H_2O)_n$; the apparent hydrogen elimination reaction takes place.[4—7,20,38,39] We have successfully elucidated this product switch in terms of the thermochemical stability of the reactants and products. But for larger n, the mass spectra have peaks at the mass of $M^+(H_2O)_n$ again. One plausible explanation of this second switch is that in the cluster magnesium is doubly charged as M^{2+} and an excess electron is on the water cluster $(H_2O)_n^-$. The present calculations, on the other hand, suggest that the chemical formula $[M(H_2O)_n]^+$ implies not only M^+ and $(H_2O)_n$ (or M^{2+} and $(H_2O)_n^-$) but also $(HOMH)^+$ and $(H_2O)_{n-1}$. In fact, in $(HOBH)^+$ the boron atom is nearly doubly charged. To examine whether the similar reactions can proceed for M = Mg and Ca, realistic computational studies are required, because this second switch is found at $n > 15$ in Mg and Ca. Definitely efficient codings, which utilise the parallel computation facility, are required.

The Strategy of the Unit of the Move in MC Samplings. We have introduced a new device in moving the atoms in every step in Monte Carlo samplings; the moves are split to rigid and non-rigid ones almost equally. This strategy is powerful to enlarge the possible conformational space we can visit under a limited number of steps, and it enables us to follow the intra-cluster reactions. At any move the same energy threshold is used, independently of rigid-move and non-rigid moves.

MC versus MD. After Car and Parinello's pioneer works, ab initio molecular dynamics (MD) has become very popular, particularly combined with plane-wave expansion

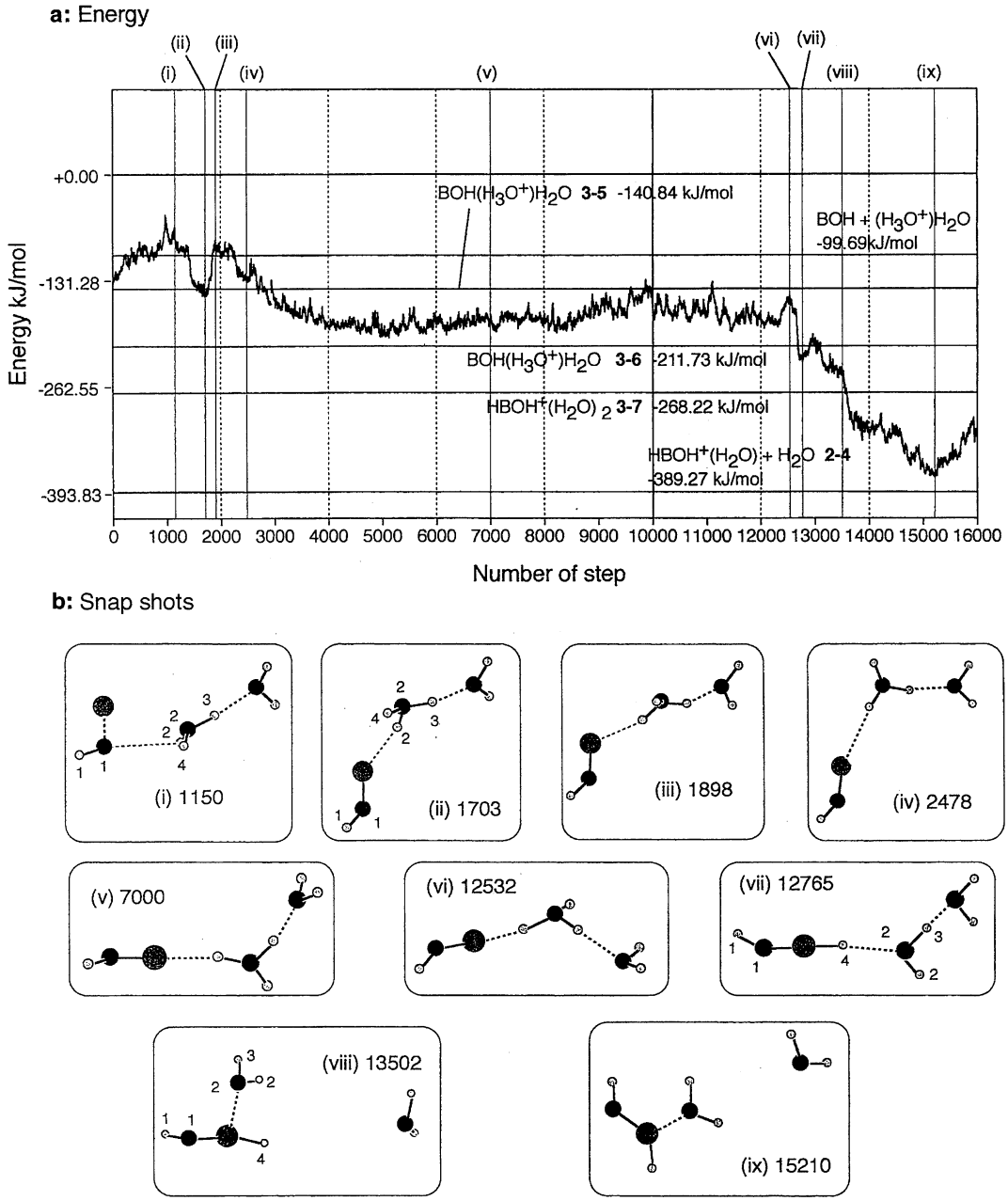

Fig. 10. Energy profile (a) and structures of some intermediate steps (b). The sampling starts at structure **3-5**, in which $H_5O_2^+$ ion is bonded to the neutral BOH molecule.

density functional theory. Because ab initio MO MD with the ordinal Gaussian expansion is very time-consuming, almost no practical applications are reported, though several test calculations were attempted. In the MD procedure, the energy gradient for all atoms at every step is required. In our work we have selected the MC method, at first to avoid the energy gradient calculations. But, it turns out that the MC method is the right choice. With ordinal ab initio MO methods, the Hartree–Fock (SCF) method based on a single determinant wave function can apply only near the equilibrium conformation. If one of the bond lengths is much longer than the equilibrium distance, the quality of the wave function is deteriorated and, as a result, the calculated energy becomes high. Besides, the curvature is positive and large and thus, the bond is shortened. Therefore, if we use the MD combined with ab initio SCF MO, we could never find the intracluster reactions. On the other hand, in the MC samplings, if the energy becomes high at longer bond distance, the sampling is rejected under the Metropolis criteria. In MC the displacement of the coordinates is finite and it is often adjusted during the sampling procedure so that the acceptance rate is 50%. In the present study, the maximum displacement is 0.5A. This rather large displacement does allow the proton transfer reaction to take place. But, this apparent advantage of the present procedure is again somewhat dangerous, particularly if the real static properties are evaluated.

The authors acknowledge Prof. Okamoto and Dr. Handsmann in our Institute for helpful discussion. H.W. thanks Research Fellowships of the Japan Society for the Promotion of Science for Young Scientists for the financial supports. T.A. was a fellows of the Institute for Molecular Science.

References

1) K. Fuke, F. Misaizu, M. Sanekata, K. Tsukamoto, and S. Iwata, *Z. Phys. D-Atoms, Molecules and Clusters*, **26S**, 180 (1993).
2) F. Misaizu, K. Tsukamoto, M. Sanekata, and K. Fuke, *Chem. Phys. Lett.*, **188**, 241 (1992).
3) F. Misaizu, K. Tsukamoto, M. Sanekata, and K. Fuke, *Z. Phys. D-Atoms, Molecules and Clusters*, **26**, 177 (1993).
4) F. Misaizu, M. Sanekata, M. Tsukamoto, K. Fuke, and S. Iwata, *J. Phys. Chem.*, **92**, 8259 (1992).
5) M. Sanekata, F. Misaizu, K. Fuke, S. Iwata, and K. Hashimoto, *J. Am. Chem. Soc.*, **117**, 747 (1995).
6) M. Sanekata, F. Misaizu, and K. Fuke, *J. Chem. Phys.*, **104**, 9768 (1996).
7) F. Misaizu, M. Sanekata, K. Fuke, and S. Iwata, *J. Chem. Phys.*, **100**, 1161 (1994).
8) C. S. Yeh, K. F. Willey, D. L. Robbins, J. S. Pilgrim, and M. A. Duncan, *Chem. Phys. Lett.*, **196**, 233 (1992).
9) K. F. Willey, C. S. Yeh, D. L. Robbins, J. S. Pilgrim, and M. A. Duncan, *J. Phys. Chem.*, **96**, 8886 (1992).
10) K. F. Willey, C. S. Yeh, D. L. Robbins, and M. A. Duncan, *J. Phys. Chem.*, **96**, 7833 (1992).
11) C. T. Scurlock, S. H. Pullins, J. E. Reddic, and M. A. Duncan, *J. Chem. Phys.*, **104**, 4591 (1996).
12) I. V. Hertel, C. Hüglin, C. Nitsch, and C. P. Schultz, *Phys. Rev. Lett.*, **67**, 1767 (1991).
13) C. P. Schultz, R. Haugstätter, H. U. Tittes, and I. V. Hertel, *Z. Phys. D-Atoms, Molecules and Clusters*, **10**, 279 (1988).
14) C. J. Weinheimer and J. M. Lizy, *J. Chem. Phys.*, **105**, 2938 (1996).
15) M. H. Shen, J. W. Winniczek, and J. M. Farrar, *J. Phys. Chem.*, **91**, 6447 (1987).
16) M. H. Shen and J. M. Farrar, *J. Phys. Chem.*, **93**, 4386 (1989).
17) M. H. Shen and J. M. Farrar, *J. Chem. Phys.*, **94**, 3322 (1991).
18) S. G. Donnelly and J. M. Farrar, *J. Chem. Phys.*, **98**, 5450 (1993).
19) C. A. Schmuttenmaer, J. Quan, S. G. Donnelly, M. J. DeLuca, D. F. Varley, L. A. DeLouise, R. J. D. Millar, and J. M. Farrar, *J. Phys. Chem.*, **97**, 3077 (1993).
20) A. C. Harms, S. N. Khanna, B. Chen, and A. W. Castleman, Jr., **100**, 3540 (1994).
21) M. Beyer, C. Berg, H. W. Görlitizer, T. Schindler, U. Achatz, G. Albert, G. Niedner-Schatteburg, and V. E. Bondybey, *J. Am. Chem. Soc.*, **118**, 7386 (1996).
22) H. Watanabe, M. Aoki, and S. Iwata, *Bull. Chem. Soc. Jpn.*, **66**, 3245 (1993).
23) M. Sodupe, C. W. Bauschlicher, Jr., and H. Partridge, *Chem. Phys. Lett.*, **181**, 321 (1991).
24) J. Hrusák, D. Stöckigt, and H. Schwarz, *Chem. Phys. Lett.*, **221**, 518 (1994).
25) C. W. Bauschlicher, Jr., and H. Partridge, *J. Phys. Chem.*, **95**, 9694 (1991).
26) H. Watanabe and S. Iwata, *J. Phys. Chem.*, **100**, 3377 (1996).
27) J. E. Jones, *Proc. R. Soc. A*, **105**, 463 (1924).
28) R. A. Buckingham, *Proc. R. Soc. A*, **168**, 264 (1938).
29) O. Matsuoka, E. Clementi, and M. Yoshimine, *J. Chem. Phys.*, **64**, 1351 (1976).
30) W. L. Jorgensenm, J. Chandrasekher, J. D. Madura, R. W. Impey, and M. L. Klein, *J. Chem. Phys.*, **79**, 926 (1983).
31) K. Laasonen, M. Parrinello, R. Car, C. Lee, and D. Vanderbilt, *Chem. Phys. Lett.*, **207**, 208 (1993).
32) T. Asada and S. Iwata, *Chem. Phys. Lett.*, **260**, 1 (1996).
33) H. Watanabe and S. Iwata, in preparation.
34) S. Sakamoto and F. Yonezawa, *Solid State Phys.*, **24**, 219 (1989).
35) S. F. Boys and F. Bernardi, *Mol. Phys.*, **21**, 533 (1970).
36) "Gaussian 92, Revision E.2," M. J. Frisch, G. W. Trucks, M. Head-Gordon, P. M. W. Gill, M. W. Wong, J. B. Foresman, B. G. Johnson, H. B. Schlegel, M. A. Robb, E. S. Replogle, R. Gomperts, J. L. Andres, K. Raghavachari, J. S. Binkley, C. Gonzalez, R. L. Martin, D. J. Fox, D. J. Defrees, J. Baker, J. J. P. Stewart, and J. A. Pople, Gaussian, Inc., Pittsburgh, PA (1992).
37) "Gaussian 94, Revision B.2," M. J. Frisch, G. W. Trucks, H. B. Schlegel, P. M. W. Gill, B. G. Johnson, M. A. Robb, J. R. Cheeseman, T. Keith, G. A. Petersson, J. A. Montgomery, K. Raghavachari, M. A. Al-Laham, V. G. Zakrzewski, J. V. Ortiz, J. B. Foresman, J. Cioslowski, B. B. Stefanov, A. Nanayakkara, M. Challacombe, C. Y. Peng, P. Y. Ayala, W. Chen, M. W. Wong, J. L. Andres, E. S. Replogle, R. Gomperts, R. L. Martin, D. J. Fox, J. S. Binkley, D. J. Defrees, J. Baker, J. P. Stewart, M. Head-Gordon, C. Gonzalez, and J. A. Pople, Gaussian, Inc., Pittsburgh, PA (1995).
38) H. Watanabe, S. Iwata, K. Hashimoto, K. Fuke, and F. Misaizu, *J. Am. Chem. Soc.*, **117**, 755 (1995).
39) H. Watanabe and S. Iwata, *J. Phys. Chem. A*, **101**, 487 (1997).
40) D. Feller, E. D. Glendening, R. A. Kendall, and K. A. Peterson, *J. Chem. Phys.*, **100**, 4981 (1994).
41) E. D. Glendening and D. Feller, *J. Phys. Chem.*, **99**, 3060 (1995).
42) E. D. Glendening and D. Feller, *J. Phys. Chem.*, **100**, 4790 (1996).
43) K. Hashimoto and K. Morokuma, *J. Am. Chem. Soc.*, **116**, 11436 (1994).
44) K. Hashimoto, S. He, and K. Morokuma, *Chem. Phys. Lett.*, **206**, 297 (1993).